$HCo(CO)_3$-Catalyzed Propene Hydroformylation. Insight into Detailed Mechanism

Chun-Fang Huo,† Yong-Wang Li,† Matthias Beller,‡ and Haijun Jiao*,†,‡

The State Key Laboratory of Coal Conversion, Institute of Coal Chemistry, Chinese Academy of Sciences, Taiyuan 030001, People's Republic of China, and Leibniz-Institut für Organische Katalyse an der Universität Rostock e.V., Buchbinderstrasse 5-6, 18055 Rostock, Germany

Received June 24, 2003

The entire catalytic cycle of propene hydroformylation using $HCo(CO)_3$ as an active catalyst has been systematically investigated at the B3LYP density functional level of theory. It is found that the most stable π-complex $HCo(CO)_3(\eta^2$-$H_2C{=}CHCH_3)$ has a C=C double bond coordination in the equatorial position, and the subsequent olefin insertion (alkylation) process is reversible, in agreement with the experimental finding. The hydride migratory insertion is accompanied by $Co(CO)_3$ pseudorotation, leading to the Co···H−C agostic stabilized (iso)propyl complex $(C_3H_7)Co(CO)_3$ with the alkyl group at the axial position and thus does not take place on a C_s symmetry potential energy surface. The regioselectivity is mainly determined by the relative stability of the alkyl cobalt tetracarbonyl complexes (C_3H_7)-$Co(CO)_4$ from the exothermic and irreversible CO addition to the alkyl cobalt tricarbonyl complexes $(C_3H_7)Co(CO)_3$, which is therefore a thermodynamic controlled process. The CO insertion process (carbonylation) proceeds via two $Co(CO)_3$ pseudorotated transition states and a Co···H−C agostic stabilized intermediate. The resulting most stable complex $(C_3H_7$-$CO)Co(CO)_3$ with the acyl group in the axial site has a η^2-O=C interaction at the equatorial site, and the computed characteristic vibrational modes agree well with the available experimental data. In contrast to the generally accepted conclusion, H_2 coordination to the acyl complex rather than oxidative addition is the rate-determining step after $HCo(CO)_3$ generation. This finding is supported by the high stability of the acyl complex toward further H_2 addition, as found experimentally.

Introduction

As an efficient route for converting olefins and synthesis gas ($CO + H_2$) into the corresponding aldehydes, hydroformylation, or the oxo process, has become one of the most important applications of homogeneous catalysis in industry.[1−8] Along with the technical developments, over 6 million tons per year of oxo products are obtained via this method worldwide in the past decade.[1,2,8] Although several metal-based catalysts (Ru, Pt, Pd, Ir, or Os) are utilized on a laboratory scale, e.g., in asymmetric hydroformylation,[9] the main interest in industry and academic research focuses on Co- and Rh-based catalysts.[1] On a commercial scale Rh catalysts have become the catalysts of choice for hydroformylation of small alkenes (C3−C6). Nevertheless a significant number of aldehydes are produced via cobalt catalysis. As an precatalyst $Co_2(CO)_8$ is mainly applied for hydroformylation of higher olefins. Here, predominantly the C8/C9 range (diisobutene, propene trimer) is used as feedstock.

The widely accepted Heck and Breslow[10] mechanism for Co-based hydroformylation reaction (Scheme 1) consists of seven elementary steps: (i) catalyst generation, (ii) olefin coordination, (iii) olefin insertion, (iv) CO addition, (v) CO insertion, (vi) H_2 oxidative addition, and (vii) aldehyde reductive elimination with catalyst regeneration. The experimental evidence suggests that, after $HCo(CO)_3$ generation, H_2 oxidative addition is the rate-determining step.[11,12] Because the insertion of the olefin into the Co−H bond can occur in two ways, Markovnikov and *anti*-Markovnikov, the products are usually mixtures of linear and branched isomers.[13] For conventional applications aimed at plasticizer alcohols, *anti*-Markovnikov orientation leading to linear aldehydes is preferred. However, the latest research re-

* Corresponding author. E-mail: hjiao@ifok.uni-rostock.de.
† Chinese Academy of Sciences.
‡ Leibniz-Institut für Organische Katalyse an der Universität Rostock e.V.

(1) (a) van Leeuwen, P. W. N. M.; Claver, C. *Rhodium Catalyzed Hydroformylation*; Kluwer Academic Publishers: Dordrecht, Netherlands, 2000. (b) Falbe, J. *New Sytheses with Carbon Monoxide*; Springer-Verlag: Berlin, 1980. (c) Torrent, M.; Solà, M.; Frenking, G. *Chem. Rev.* **2000**, *100*, 439.
(2) Beller, M.; Cornils, B.; Frohning, C. D.; Kohlpaintner, C. W. *J. Mol. Catal. A* **1995**, *104*, 17.
(3) Parshall, G. W.; Ittel, S. D. *Homogeneous Catalysis*; Wiley-Interscience: New York, 1992.
(4) Cornils, B.; Herrmann, W. A. *Applied Homogeneous Catalysis with Organometallic Compounds*; Wiley-VCH: Weinheim, 2002; Vol. 1.
(5) Heck, R. F. *Adv. Organomet. Chem.* **1966**, *4*, 243.
(6) Orchin, M.; Rupilius, W. *Catal. Rev.* **1972**, *6*, 85.
(7) Süss-Fink, G.; Meister, G. *Adv. Organomet. Chem.* **1993**, *35*, 41.
(8) Papadogianakis, G.; Sheldon, R. A. *New J. Chem.* **1996**, *20*, 175.
(9) Agbossou, F.; Carpentier, J.-F.; Mortreux, A. *Chem. Rev.* **1995**, *95*, 2485.
(10) Heck, R. F.; Breslow, D. S. *J. Am. Chem. Soc.* **1961**, *83*, 4023.
(11) Dombeck, D. *Adv. Catal.* **1983**, *32*, 325.
(12) Feng, J.; Garland, M. *Organometallics* **1999**, *18*, 417.
(13) Crabtree, R. H. *The Organometallic Chemistry of the Transition Metals*; Wiley: New York, 1988.

10.1021/om0304863 CCC: $25.00
Publication on Web 10/17/2003

Scheme 1. Heck and Breslow Hydroformylation Mechanism

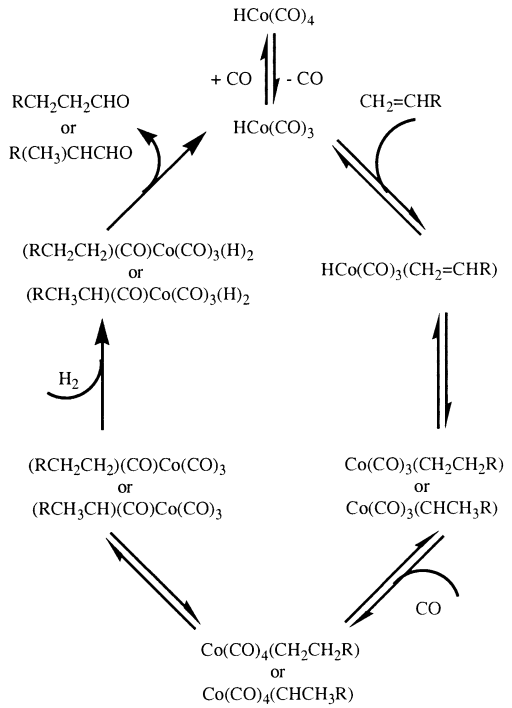

vealed that branched optical pure aldehydes are also valuable precursors for pharmaceuticals and agrochemicals.[2]

Due to its industrial importance, hydroformylation has received considerable attention both experimentally[14−31] and theoretically.[32−53] A two-phase system[14] or supercritical carbon dioxide[15−17] as reaction medium has improved the product separation situation. Even so, the main research activities in this field are focused on ligand-modified catalysts for obtaining high regioselectivity.[2,22,23] Therefore, understanding the mechanism in detail and unraveling the origin of regioselectivity are very crucial. The development of computational techniques, ab initio molecular orbital theory and in particular density functional theory (DFT), has made the understanding of detailed mechanisms at the molecular level possible.[32]

The mechanism of hydroformylation with Rh-based catalysts has been investigated extensively by computational methods. Frenking et al. explored a series of elementary reactions with $HRh(CO)_4$ catalyst[33] and a phosphine-modified Rh-based catalyst.[34] In addition, Koga et al.,[35,36] Musaev et al.,[37] and Matsubara et al.[38] examined the $HRh(PH_3)(CO)_2$-catalyzed ethylene hydroformylation at the MP2//HF level. Recently, ethylene hydroformylation catalyzed by $HRh(PH_3)_2(CO)$ was mapped out at the DFT level by Decker and Cundari.[39]

For Co-based hydroformylation, although considerable efforts have been made, they were carried out at various levels of theory. The first theoretical investigation on propene hydroformylation was carried out by Grima et al. with the CNDO method and at a low ab initio level of theory more than 25 years ago (1976),[41] and this study analyzed the elementary step of propene insertion and the influence of the electronic factors on the regioselectivity. Ten years later, Antolovic and Davidson[42] studied the electronic structures of some cobalt carbonyl complexes involved in the catalytic cycle of hydroformylation. At the Hartree−Fock Slater (HFS) and BP86 density functional levels, Ziegler et al.[43,45,47,48] studied the intermediates and transition states for each elementary step. However, most of these studies were limited due to the computational deficiencies at that time (partial optimization, insufficient basis set, no characterization of ground and transition states, no electron correlation, and a brief comparison with our new results is given later), but they contributed to understand the catalytic cycle in Scheme 1 in a reasonable way. More recently, the study on CO insertion reaction of (CH_3)-$Co(CO)_4$ was reported by Goh and Marynick[46] at the B3LYP DFT level.

With the increase in knowledge of hydroformylation, the exploration of regioselectivity is attracting more and more attention. For Rh-catalyzed reactions, it is verified that the regioselectivity is controlled by irreversible olefin insertion reaction.[24] On this basis, some groups studied insertion reactions of terminal olefins other than

(14) Beller, M.; Krauter, J. G. E. *J. Mol. Catal. A* **1999**, *143*, 31.
(15) Rathke, J. W.; Klingler, R. J.; Krause, T. R. *Organometallics* **1991**, *10*, 1350.
(16) Guo, Y.; Akgerman, A. *Ind. Eng. Chem. Res.* **1997**, *36*, 4581.
(17) Ke, J.; Han, B.; George, M. W.; Yan, H.; Poliakoff, M. *J. Am. Chem. Soc.* **2001**, *123*, 3661.
(18) Piacenti, F.; Calderazzo, F.; Bianchi, M.; Rosi, L.; Frediani, P. *Organometallics* **1997**, *16*, 4235.
(19) Rode, E. J.; Davis, M. E.; Hanson, B. E. *J. Catal.* **1985**, *96*, 563.
(20) Rode, E. J.; Davis, M. E.; Hanson, B. E. *J. Catal.* **1985**, *96*, 574.
(21) Woo, S. I.; Hill, C. G., Jr. *J. Mol. Catal.* **1985**, *29*, 231.
(22) Casey, C. P.; Paulsen, E. L.; Beuttenmueller, E. W.; Proft, B. R.; Petrovich, L. M.; Matter, B. A.; Powell, D. R. *J. Am. Chem. Soc.* **1997**, *119*, 11817.
(23) Paciello, R.; Siggel, L.; Röper, M. *Angew. Chem., Int. Ed.* **1999**, *38*, 1920.
(24) Casey, C. P.; Petrovich, L. M. *J. Am. Chem. Soc.* **1995**, *117*, 6007.
(25) Massick, S. M.; Rabor, J. G.; Elbers, S.; Marhenke, J.; Bernhard, S.; Schoonover, J. R.; Ford, P. C. *Inorg. Chem.* **2000**, *39*, 3098.
(26) Beller, M.; Zimmermann, B.; Geissler, H. *Chem. Eur. J.* **1999**, *5*, 1301.
(27) Selent, D.; Wiese, K.-D.; Röttger, D.; Börner, A. *Angew. Chem.* **2000**, *112*, 1694; *Angew. Chem., Int. Ed.* **2000**, *39*, 1639.
(28) Breit, B.; Seiche, W. *Synthesis* **2001**, 1.
(29) van der Veen, L. A.; Kamer, P. C. J.; van Leeuwen, P. W. N. M. *Angew. Chem.* **1999**, *111*, 349; *Angew. Chem., Int. Ed.* **1999**, *38*, 336.
(30) Klein, H.; Jackstell, R.; Wiese, K.-D.; Beller, M. *Angew. Chem.* **2001**, *113*, 3505; *Angew. Chem. Int. Ed.* **2001**, *40*, 3408.
(31) Selent, D.; Hess, D.; Wiese, K.-D.; Röttger, D.; Kunze, C.; Börner, A. *Angew. Chem.* **2001**, *113*, 1739; *Angew. Chem., Int. Ed.* **2001**, *40*, 1696.
(32) Niu, S.; Hall, M. B. *Chem. Rev.* **2000**, *100*, 353.
(33) Pidun, U.; Frenking, G. *Chem. Eur. J.* **1998**, *4*, 522.
(34) Schmid, R.; Herrmann, W. A.; Frenking, G. *Organometallics* **1997**, *16*, 701.
(35) Koga, N.; Jin, S. Q.; Morokuma, K. *J. Am. Chem. Soc.* **1988**, *110*, 3417.
(36) Koga, N.; Morokuma, K. *Top. Phys. Organomet. Chem.* **1989**, *3*, 1.
(37) Musaev, D. G.; Matsubara, T.; Mebel, A. M.; Koga, N.; Morokuma, K. *Pure Appl. Chem.* **1995**, *67*, 257.
(38) Matsubara, T.; Koga, N.; Ding, Y.; Musaev, D. G.; Morokuma, K. *Organometallics* **1997**, *16*, 1065.
(39) Decker, S. A.; Cundari, T. R. *Organometallics* **2001**, *20*, 2827.
(40) Rossi, A. R.; Hoffmann, R. *Inorg. Chem.* **1975**, *14*, 365.
(41) Grima, J. Ph.; Choplin, F.; Kaufmann, G. *J. Organomet. Chem.* **1977**, *129*, 221.
(42) Antolovic, D.; Davidson, E. R. *J. Am. Chem. Soc.* **1987**, *109*, 5828.
(43) Versluis, L.; Ziegler, T.; Fan, L. *Inorg. Chem.* **1990**, *29*, 4530.
(44) Berke, H.; Hoffmann, R. *J. Am. Chem. Soc.* **1978**, *8*, 7224.
(45) Versluis, L.; Ziegler, T.; Baerends, E. J.; Ravenek, W. *J. Am. Chem. Soc.* **1989**, *111*, 2018.
(46) Goh, S. K.; Marynick, D. S. *Organometallics* **2002**, *21*, 2262.
(47) Versluis, L.; Ziegler, T. *Organometallics* **1990**, *9*, 2985.
(48) Solà, M.; Ziegler, T. *Organometallics* **1996**, *15*, 2611.

ethylene catalyzed by Rh complexes.[50,51] Furthermore, in the latest experimental[23] and theoretical work,[52,53] the electronic and steric (bite angle) effects on regioselectivity in phosphine-modified Rh-catalyzed hydroformylation have also been examined. However, for the regioselectivity of Co-catalyzed hydroformylation processes, less information is known of the theoretical aspects.

In this paper, the potential energy surface (PES) of the full cycle of propene hydroformylation catalyzed by $HCo(CO)_3$ has been investigated at the B3LYP density functional level of theory, and the origin of regioselectivity has also been addressed. The structures of all intermediates and transition states involved in this process have been located, and the relative energies of these species have been calculated. In light of the energy profiles along the reaction path, it has been computed that H_2 coordination is the rate-determining step. The origin of regioselectivity is found to be mainly controlled by the thermodynamic stability of the alkyl cobalt tetracarbonyl complex ($RCo(CO)_4$), formed from the exothermic and irreversible CO addition on the alkyl cobalt tricarbonyl complex ($RCo(CO)_3 + CO$), and the olefin insertion (alkylation) process is found to be reversible.

Computational Details

All calculations were performed based on the B3LYP/6-311+G(d) hybrid density functional theory with the Gaussian 98 program.[54] This method is found to be appropriate for cobalt carbonyl chemistry, as indicated by the excellent agreement in vibrational frequencies and bond dissociation energies between theory and experiment,[55] and the deduced scaling factor for vibration frequencies at this level is 0.9667. The geometries of the intermediates and transition states were fully optimized, without any symmetry constraints, if not noted otherwise. The frequency calculations at the same level were also carried out to confirm that the optimized structures were ground states without imaginary frequency (NImag = 0) or transition states with one imaginary frequency (NImag = 1). Especially, the lone imaginary frequency of each transition state displayed the desired displacement orientation, and the validity of each reaction path was further examined by the intrinsic reaction coordinate calculations (IRC). Zero-point energy corrections (ZPE), derived from the frequency calculations, were added to the total energies of each species in the catalytic cycle. On the basis of the transition state theory, the reaction rates were calculated under the actual reaction condition of 403.15 K and 200 atm. The Wiberg bond indexes and natural charges were also analyzed with the natural bond orbital (NBO) program.[56] The calculated total electronic energies, ZPE, and thermal corrections to enthalpies and Gibbs free energies (403.15 K and 200 atm) as well as natural charges and vibration frequencies are provided in the Supporting Information.

The following notations are used to represent the different types of complexes involved in each elementary reaction throughout the text. For example, **1a-*syn***, **1b-*anti***, **1c-*syn***, and **1d-*anti*** are the rotational isomers of the π-complex $HCo(CO)_3(\eta^2\text{-}H_2C{=}CHCH_3)$. The alkyl tri- and tetracarbonyl complexes ($(C_3H_7)Co(CO)_3$ and $(C_3H_7)Co(CO)_4$) are designed as **2L/2B** and **3L/3B**, in which **L** and **B** mean the pathways for linear (*anti*-Markovnikov) and branched (Markovnikiv) products. For the acyl cobalt tricarbonyl complexes $(C_3H_7CO)Co(CO)_3$, **4L-H/4B-H** and **4L-O/4B-O** represent the Co···H−C agostic and η^2-O=C stabilized intermediates, and their corresponding complexes $(C_3H_7CO)Co(CO)_3(\eta^2\text{-}H_2)$ from H_2 coordination are denoted as **5Lb/5Bb** and **5La/5Ba**. Their dihydride complexes $(C_3H_7CO)Co(CO)_3(H)_2$ from H_2 oxidative addition are noted as **6L/6B**, and **7L/7B** are the aldehyde adducts with the active catalyst, $HCo(CO)_3(C_3H_7CHO)$. In addition, **5Lc/5Bc** represent the acyl cobalt tetracarbonyl complex $(C_3H_7CO)Co(CO)_4$ as the side reaction products. The authentic transition state is denoted as **TS** in combination with the notations of the corresponding reactant and product.

Results and Discussion

(a) Catalyst Generation. The first key step in the mechanism of Heck and Breslow[10] is the formation of the 16-electron unsaturated active catalyst species, $HCo(CO)_3$, via CO dissociation from $HCo(CO)_4$. The structure and bonding of these two complexes have been investigated extensively at various levels of theory. As found in our latest work,[55] $HCo(CO)_3$ has a C_{2v} planar structure representing the most stable singlet state. The loss of the equatorial CO from $HCo(CO)_4$ is the only energetically favored pathway, and other higher energetic alternatives are not competitive.[55]

(b) Olefin Coordination. In light of the planar $HCo(CO)_3$ conformation, there are two orientations for the propene C=C bond coordination: (i) perpendicular to the axial Co−H bond and (ii) parallel to the axial Co−H bond. The optimized structures with the Newman projection and relative energies are shown in Figure 1.

Due to the orientation of the methyl group in propene, there are two isomers for each type of complex; that is, the methyl group is located at the same side as (*syn*) or at the opposite side from (*anti*) the Co−H bond (other enantiomers are not shown here). For type (i) complexes, the *syn* (**1a-*syn***) and the *anti* (**1b-*anti***) isomers are isoenergetic with less than 0.2 kJ/mol. The energy difference of the two isomers of type (ii) complexes, **1c-*syn*** and **1d-*anti***, is also very small (0.6 kJ/mol). However, **1a-*syn*** and **1b-*anti*** are more favored than **1c-*syn*** and **1d-*anti*** by 16−17 kJ/mol. Apart from the proposed qualitative orbital interaction of donation and back-donation by Versluis et al.,[43] this energy difference can be of steric origin, since the distances between cobalt and the C=C bond in **1c-*syn*** and **1d-*anti*** (2.282/2.341 vs 2.269/2.357 Å) are longer than those in **1a-*syn*** and

(49) Versluis, L.; Ziegler, T. *J. Am. Chem. Soc.* **1990**, *112*, 6763.
(50) Alagona, G.; Ghio, C.; Lazzaroni, R.; Settambolo, R. *Organometallics* **2001**, *20*, 5394.
(51) Rocha, W. R.; De Almeida, W. B. *Int. J. Quantum Chem*. 2000, *78*, 42.
(52) Gleich, D.; Schmid, R.; Herrmann, W. A. *Organometallics* **1998**, *17*, 4828.
(53) Carbó, J. J.; Maseras, F.; Bo, C.; van Leeuwen, P. W. N. M. *J. Am. Chem. Soc.* **2001**, *123*, 7630.
(54) Frisch, M. J.; Trucks, G. W.; Schlegel, H. B.; Scuseria, G. E.; Robb, M. A.; Cheeseman, J. R.; Zakrzewski, V. G.; Montgomery, J. A.; Stratmann, R. E.; Burant, J. C.; Dapprich, S.; Millam, J. M.; Daniels, A. D.; Kudin, K. N.; Strain, M. C.; Farkas, O.; Tomasi, J.; Barone, V.; Cossi, M.; Cammi, R.; Mennucci, B.; Pomelli, C.; Adamo, C.; Clifford, S.; Ochterski, J.; Petersson, G. A.; Ayala, P. Y.; Cui, Q.; Morokuma, K.; Malick, D. K.; Rabuck, A. D.; Raghavachari, K.; Foresman, J. B.; Cioslowski, J.; Ortiz, J. V.; Stefanov, B. B.; Liu, G.; Liashenko, A.; Piskorz, P.; Komaromi, I.; Gomperts, R.; Martin, R. L.; Fox, D. J.; Keith, T.; Al-Laham, M. A.; Peng, C. Y.; Nanayakkara, A.; Gonzalez, C.; Challacombe, M.; Gill, P. M. W.; Johnson, B. G.; Chen, W.; Wong, M. W.; Andres, J. L.; Head-Gordon, M.; Replogle E. S.; Pople, J. A. *Gaussian 98* (Revision A.1); Gaussian, Inc.: Pittsburgh, PA, 1998.
(55) Huo, C.-F.; Li, Y.-W.; Wu, G.-S.; Beller, M.; Jiao, H. *J. Phys. Chem. A* **2002**, *106*, 12161.
(56) (a) Glendening, E. D.; Reed, A. E.; Carpenter, J. E.; Weinhold, F. *NBO* Version 3.1. (b) Reed, A. E.; Curtiss, L. A.; Weinhold, F. *Chem. Rev*. **1988**, *88*, 899.

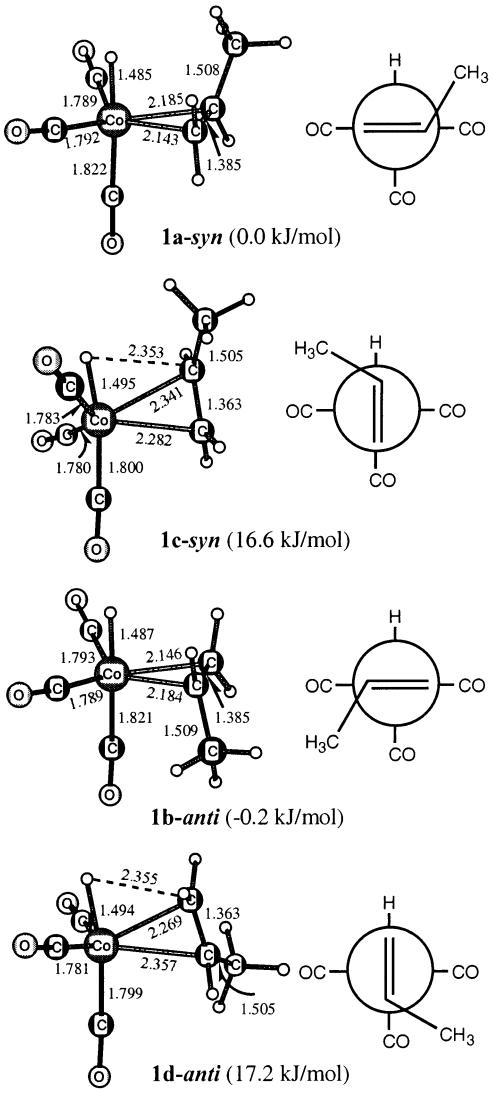

Figure 1. Bond parameters (Å), relative energies, and the Newman projection for $HCo(CO)_3(\eta^2\text{-}H_2C{=}CHCH_3)$.

1b-*anti* (2.143/2.185 vs 2.146/2.184 Å). In the most stable **1a-*syn*** and **1b-*anti***, the H−Co−C_{axial} angles are 177.7° and 176.9°, and they are less bent than those of **1c-*syn*** (168.5°) and **1d-*anti*** (167.9°) by about 9°. This indicates once again the steric interaction between the parallel Co−H and C=C bonds in **1c-*syn*** and **1d-*anti***, in which the H···C distances are 2.353 and 2.355 Å. In addition, the Co−H and C=C bonds in **1c-*syn*** and **1d-*anti*** are in close position, which facilitates the subsequent migratory insertion of η^2-$H_2C{=}CHCH_3$ into the Co−H bond.

Due to the small energy difference between the equatorial and axial complexes, we have analyzed their interconversion through the rotation of propene on the basis of the Newman projection. The potential energy profile in the flexible rotor approximation is illustrated in Figure 2. There are two minima with θ around −90° (270°) and 90° corresponding to **1a-*syn*** and **1b-*anti***, and two maxima with θ close to −20° and 150° corresponding to the transition states from **1a-*syn*** to **1c-*syn*** and **1b-*anti*** to **1d-*anti***, which are designated as **TS-(1a/1c)** and **TS(1b/1d)**. However, the related local minima with θ close to 0° and 180° correspond to **1c-*syn*** and **1d-*anti***, and the transition states for **1c-*syn*** to **1b-*anti*** (**TS(1c/1b)**) and **1a-*syn*** to **1d-*anti*** (**TS(1a/1d)**) with very small shoulder in energy are not easy to identify.

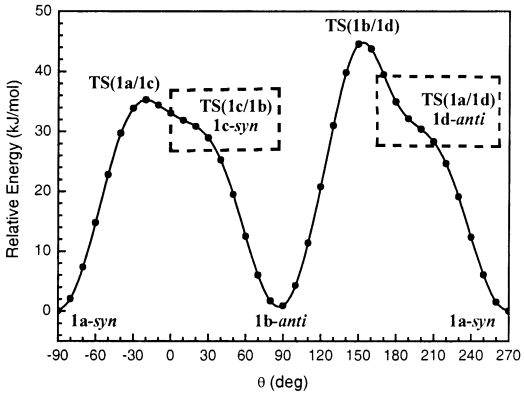

Figure 2. Potential energy profile of propene rotation (see Figure 1).

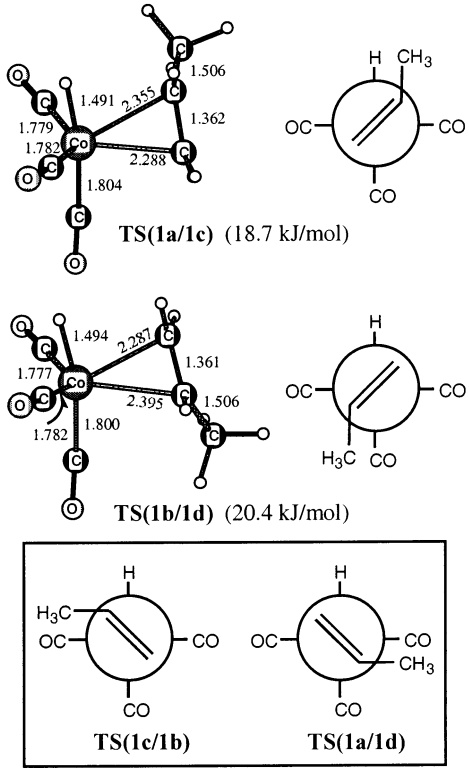

Figure 3. Bond parameters (Å), relative energies, and the Newman projection for the propene rotation transition states of $HCo(CO)_3(\eta^2\text{-}H_2C{=}CHCH_3)$.

To validate the scanned results, the transition state search has been performed. As expected, we found two transition states with only one imaginary frequency for each, indicating the rotation mode of η^2-propene, **TS-(1a/1c)** and **TS(1b/1d)**, as shown in Figure 3, and the related barriers are 18.7 and 20.6 kJ/mol. The other two transition states, **TS(1c/1b)** and **TS(1a/1d)**, are not located, but they must be close in energy as **1c-*syn*** and **1d-*anti***. Thus, one can expect free rotation of the η^2-propene ligand in the π-complexes under the actual reaction conditions.

(c) Olefin Insertion. The insertion of terminal olefins, except for ethylene, into the Co−H bond can occur in two ways, which are described as *anti*-Mark-

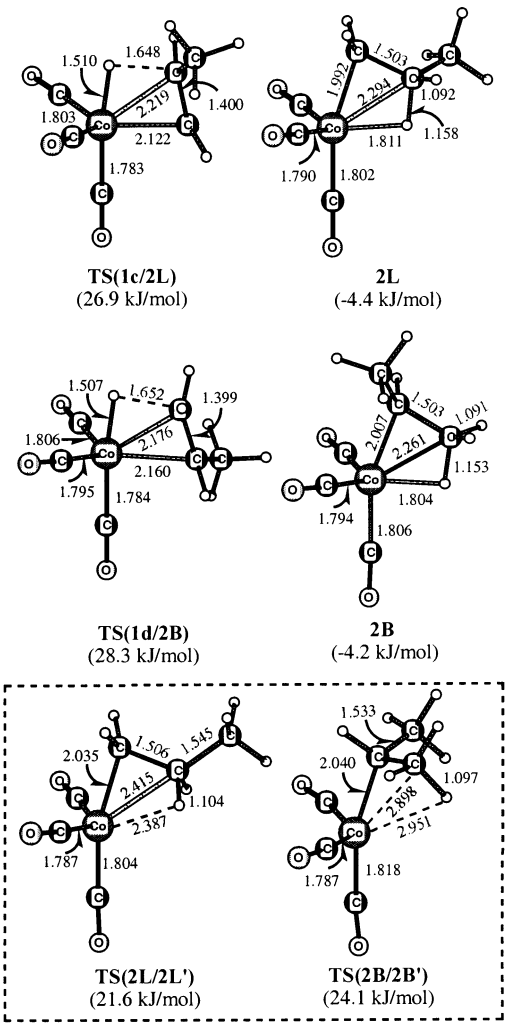

Figure 4. Bond parameters (Å) and relative energies for the transition states and products of the olefin insertion step, and the transition states for the degenerate enantiomerization.

ovnikov and Markovnikov additions. Therefore, two types of alkyl complexes, linear and branched (therefore **L** and **B** notations are used in the text), can be formed. This alkylation reaction was considered as the key step for the regioselectivity.[41] As shown in Figure 4, the structures of the two authentic transition states, **TS(1c/2L)** and **TS(1d/2B)**, are very similar to those of their π-complexes, **1c-*syn*** and **1d-*anti***. The imaginary vibration mode indicates the migratory insertion of hydrogen into the C=C double bond, and the major change in the transition states is the shortening of the H···C distances.

Similar to the π-complex, the skeleton of the transition state structure remains a distorted trigonal bipyramidal conformation, but both are different from that of the alkyl species (**2L** and **2B**). The IRC calculation shows that, after the transition state, the migration of a hydrogen atom to propene to form the (iso)propyl group is accompanied by a simultaneous rotation of the $Co(CO)_3$ group. The net effect is that only structures (**2L** and **2B**) with the (iso)propyl group in the axial site are minima on the PES of $(C_3H_7)Co(CO)_3$. They are stabilized by an additional Co···H−C agostic interaction at the formally vacant equatorial site of cobalt. To further verify this conclusion, the optimizations starting from the geometries with the (iso)propyl group in the equatorial site were performed. The results show that this kind of optimization eventually leads to the stable conformations (**2L** and **2B**). This agrees with the results by Goh and Marynick for $(CH_3CO)Co(CO)_3$[46] and by Huo et al. for $(HCO)Co(CO)_3$.[55]

As shown in Figures 1 and 4 (see also Figure 10), both migratory insertion steps (**1c-*syn*** to **2L** and **1d-*anti*** to **2B**) have close activation energies of 10.3 and 11.1 kJ/mol, and the overall activation energies for the whole insertion reaction, **1b-*anti*** to **2L** and **1a-*syn*** to **2B**, are 27.1 and 28.3 kJ/mol, respectively, in line with the experimental value of 25−33 kJ/mol determined for $[(\eta^5\text{-}C_5H_5)(P(OMe)_3)Co(C_2H_4)(\mu\text{-}H)]^+$.[57] Furthermore, the linear intermediate **2L** is slightly more stable than the branched intermediate **2B** by 0.2 kJ/mol. These small energy differences cannot be responsible for the regioselectivity, since the olefin insertion reaction is reversible rather than irreversible, as found experimentally. In addition, we located two authentic transition states, **TS(2L/2L′)** and **TS(2B/2B′)**, for the degenerated enantiomerization, indicating that the path needs 26.0 or 28.3 kJ/mol energy to break the agostic interaction.

In the study on the $HCo(CO)_3$-catalyzed propene hydroformylation, Grima et al.[41] analyzed the migratory insertion for C=C into the Co−H bond. They proposed that the origin of the regioselectivity was due to the electrostatic dipole−dipole interaction between Co−H and C=C favoring the linear product, and the disfavored branched product was due to the higher energy required for the inversion of the olefin dipole for the proper interaction. However, our results disagree with this conclusion. As given in the Supporting Information, the natural charge distribution pattern in both transition states, **TS(1c/2L)** and **TS(1d/2B)**, does not differ significantly, and no dipole inversion can be found in **TS(1d/2B)**. In addition, the charge pattern of the transition states does not differ from their ground states. Therefore, the early proposed charge effect on the regioselectivity[41] cannot be supported by the present work.

(d) CO Addition and Insertion. The following step in the catalytic cycle is the CO addition on the coordinatively unsaturated intermediates $(C_3H_7)Co(CO)_3$ to produce the 18-electron saturated species $(C_3H_7)Co(CO)_4$. The optimized structures and relative energies (relative to the sum of the energy of the **1a-*syn*** and CO) for the linear pathway and branched pathway are displayed in Figures 5 and 6, respectively.Structures **3L** and **3B** represent the most stable conformations of linear and branched cobalt tetracarbonyl intermediates, and **3L** is 8.6 kJ/mol lower in energy than **3B**, while **2L** and **2B** differ only by 0.2 kJ/mol. This shows an interesting fact in contrast to the thermochemistry of alkanes; that is, branched isobutane is 8.4 kJ/mol more stable than linear butane. This energy difference between **3L** and **3B** can be ascribed to the steric interaction between the isopropyl group and the $Co(CO)_4$ unit, as indicated by the axial Co−C bond length, i.e., 2.111 Å in **3L** and 2.154 Å in **3B**, respectively. To support this conclusion, we have calculated $RCo(CO)_4$ (R = CH_3, $C(CH_3)_3$) and found that the alkyl to cobalt distance (C−Co) is 2.080 Å for methyl and 2.205 Å for *tert*-butyl complexes, indicating the steric interaction between Co-

(57) Brookhart, M.; Volpe, A. F. Jr.; Lincoln, D. M.; Horváth, I. T.; Millar, J. M. *J. Am. Chem. Soc.* **1990**, *112*, 5634.

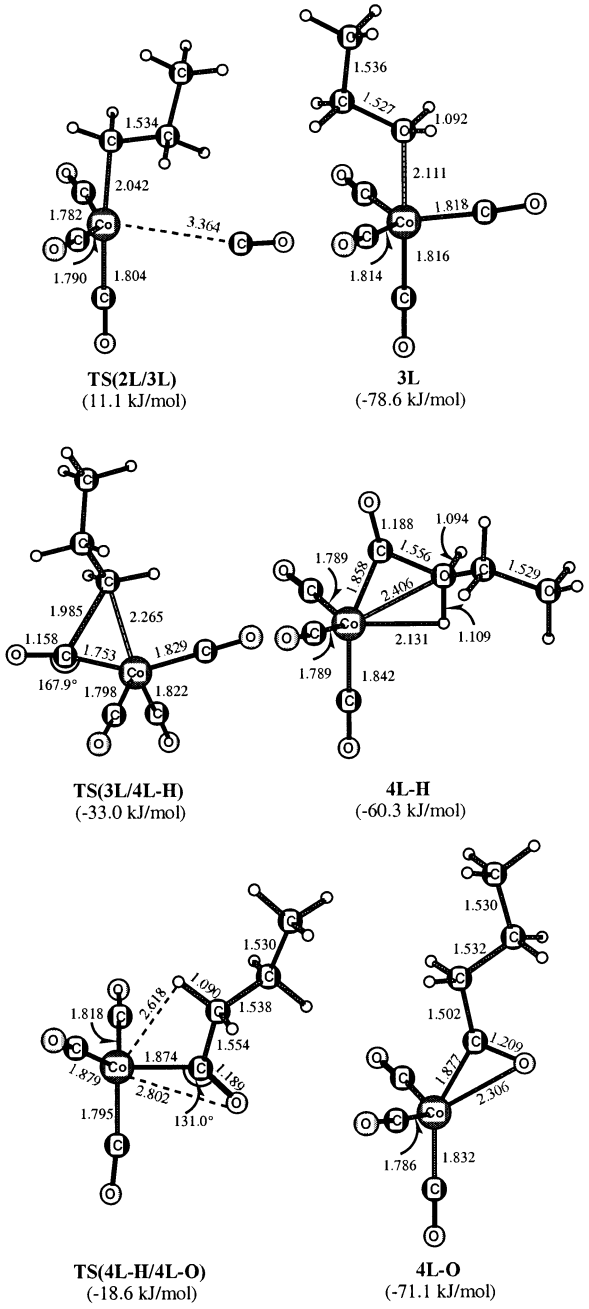

Figure 5. Bond parameters (Å) and relative energies for the intermediates and transition states of the carbonylation process for propyl (**L** for linear) substituent.

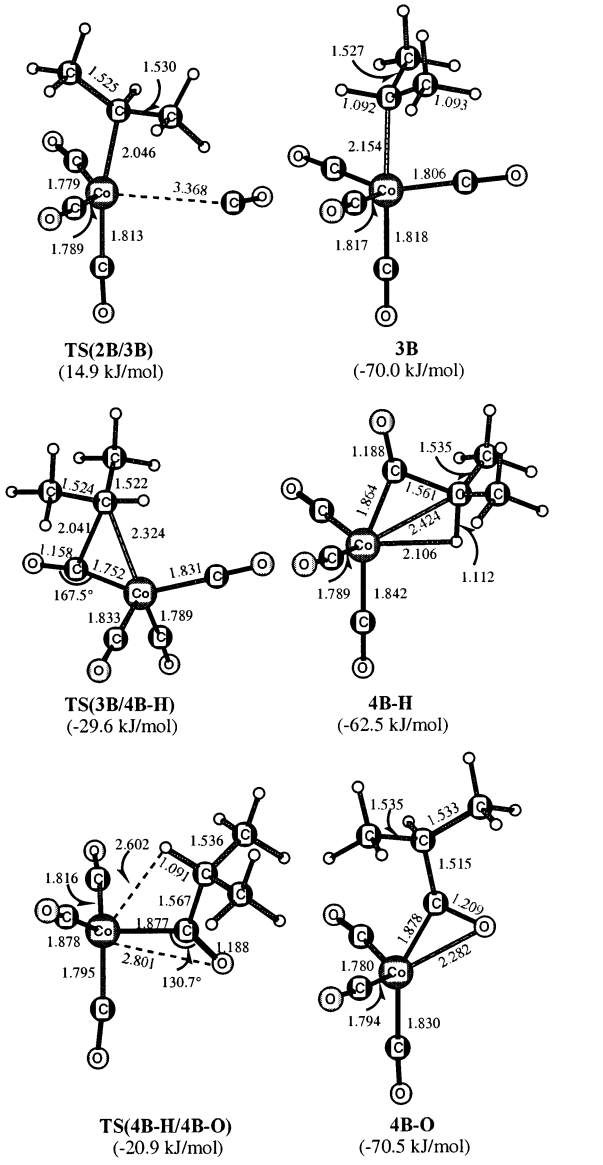

Figure 6. Bond parameters (Å) and relative energies for the intermediates and transition states of the carbonylation process for isopropyl (**B** for branched) substituent.

$(CO)_4$ and the bulky *tert*-butyl group. Moreover, CO addition to **2L** and **2B** is computed to be highly exothermic by 74.2 and 65.8 kJ/mol, and as discussed below, the thermodynamic stability of the products from this high exothermic addition should be responsible for the observed regioselectivity. To complete the energy profiles, we also have located two CO addition transition states, **TS(2L/3L)** and **TS(2B/3B)**. Since the front attack of CO to $CH_3(CO)Co(CO)_3$ was predicted to have the lowest activation energy by Goh and Marynick,[46] we studied only this possibility in our case. Despite the breaking of the agostic interaction, the calculated activation energies of 15.5 and 19.1 kJ/mol are rather small.

The next step is the CO insertion (carbonylation) process from $(C_3H_7)Co(CO)_4$ to $(C_3H_7CO)Co(CO)_3$. As illustrated in Figures 5 and 6, all conformations of acyl species have the acyl group in the axial position. One conformer is stabilized by the cobalt and hydrogen agostic (Co···H−C) interaction in the equatorial site (**4L-H** and **4B-H**), and the other has the cobalt and η^2-O=C oxygen facing the vacant site to form **4L-O** and **4B-O**. The small energy differences between **4L-H** and **4B-H**, and **4L-O** and **4B-O** of 2.2 and 0.6 kJ/mol reflect the steric origin in **3B** once again. In comparison with **4L-H** and **4B-H**, **4L-O** and **4B-O** are more stable by 10.8 and 8.0 kJ/mol, respectively. In addition, we have calculated the related vibration frequencies, which are summarized in the Supporting Information. It is to be noted that the computed CO bands for **3L** (**3B**) and $(CH_3)Co(CO)_4$ agree well with the experimental values of $(CH_3)Co(CO)_4$ after the correction to vacuum conditions.[58] The largest deviation between experiment and theory for $(CH_3)Co(CO)_4$ is only 8 cm^{-1}. For the acyl cobalt tricarbonyl complexes, the calculated η^2-acyl

(58) Sweany, R. L.; Russell, F. N. *Organometallics* **1988**, *7*, 719.

vibration band of 1686/1674 cm^{-1} for **4L-O**/**4B-O** accords with the determined η^2-O=CCH_3 vibration frequency of 1685.9 cm^{-1} by Sweany et al.[59] Moreover, the experimentally observed shift of the η^2-acyl vibration band of $(CH_3CO)Co(CO)_3$ relative to the η^1-acyl band of $(CH_3CO)Co(CO)_4$ is further reproduced by our calculations.

The carbonylation process has been investigated at various levels of theory.[42,44,45] The recent B3LYP study by Goh and Marynick[46] showed that the reaction does not proceed along a path in C_s symmetry, and the origin of such unusual (unsymmetrical) rotated migration is the result of the interaction of frontier orbitals. On this basis, we paid more attention to the process **3L** → **4L-O** (Figure 5) and **3B** → **4B-O** (Figure 6). Our study reveals that the carbonyl insertion reaction is completed in two steps. The first step is the migration of the propyl group to a c*is* carbonyl, and the second step is the transformation between the different conformers of $(C_3H_7CO)Co(CO)_3$. In the first step, **3L** → **TS(3L/4L-H)** → **4L-H** or **3B** → **TS(3B/4B-H)** → **4B-H**, the main changes are the (iso)propyl migration coupled with the skeletal change from trigonal bipyramid to strongly distorted square pyramid with the formation of a three-membered ring in the transition state and then to a butterfly conformation. The process is endothermic by 18.3 or 7.5 kJ/mol, with a barrier of 45.6 or 40.4 kJ/mol. In the transition state, **TS(3L/4L-H)** or **TS(3B/4B-H)**, the migrating propyl group forms a three-membered ring with the equatorial CO ligand as indicated by the forming C−C distance of 1.985 or 2.041 Å. The $Co-C_{propyl}$ bond is elongated (2.265 or 2.324 Å), while the Co−CO bond becomes shorter (1.753 or 1.752 Å), as compared with those of **3L** and **3B** (2.111/1.814 vs 2.154/1.806 Å). The product of the propyl migration is the Co···H−C agostic stabilized **4L-H** or **4B-H**, in which the Co···H distance is 2.131 or 2.106 Å. It is longer than that in **2L** or **2B** (1.811 or 1.804 Å).

Subsequently further isomerization of **4L-H** or **4B-H** to form the η^2-stabilized structure (**4L-O** or **4B-O)** takes place. The geometry of the corresponding transition state **TS(4L-H/4L-O)** or **TS(4B-H/4B-O)** is a distorted tetrahedron with an η^1-acyl group (Figures 5 and 6). This step is exothermic by 10.8 or 8.0 kJ/mol, with activation energy of 41.7 or 41.6 kJ/mol, respectively. The whole carbonylation process for **3L** to **4L-O** is slightly endothermic by 7.5 kJ/mol, while that for **3B** to **4B-O** is almost thermally neutral (−0.5 kJ/mol).

(e) H_2 Addition and Aldehyde Elimination. The main focus of this part is on the last step of the catalytic cycle to produce aldehyde. The source of hydrogen utilized in the aldehyde reductive elimination has been debated.[2,48] The two most plausible hydrogen sources proposed are the strong acidic $HCo(CO)_4$ species and supplied H_2. An IR spectroscopic experiment designed by Pino et al.[60] and carried out under the normal hydroformylation conditions with a H_2/D_2 mixture clearly indicated that H_2 is the main source of the hydrogen in the aldehyde elimination step, even in the presence of a large amount of $HCo(CO)_4$. Therefore, our investigations are devoted to the process where H_2 coordinates to the unsaturated acyl complex, followed by the oxidative addition of H_2 and reductive elimination of aldehydes with simultaneous recovery of the active catalyst $HCo(CO)_3$.

The existence of $RCo(CO)_3(H_2)$ species for R = H and CH_3 has been verified experimentally by Sweany and Russell[58] in inert-gas matrixes, and the hydrogen molecule was found to be coordinated and not to be oxidatively added. Here, the detailed pathways of H_2 addition and (iso)butanal elimination from $(C_3H_7CO)Co(CO)_3$ are shown in Figure 7 for the linear product and in Figure 8 for the branched isomer. The energy data in Figures 7 and 8 are relative to the sum of the energy of the **1a-*syn***, CO, and H_2.The coordination of H_2 to the unsaturated acyl cobalt complexes **4L-O** and **4B-O** or **4L-H** and **4B-H** to form the hydrogen complexes $(C_3H_7CO)Co(CO)_3(\eta^2-H_2)$, **5L** and **5B**, was investigated at first. The H_2 addition complexes are accessible from both η^2-O=C-stabilized **4L-O/4B-O** and agostic-stabilized **4L-H/4B-H.** As shown in Figures 7 and 8, we have located four H_2 addition transition states, **TS(4L-O/5La)/TS(4L-H/5Lb)** and **TS(4B-O/5Ba)/TS(4B-H/5Bb)**, for linear and branched pathways, and the calculated addition barriers are 26.1/26.9 and 29.9/32.7 kJ/mol, respectively. In these transition states, H_2 attaches the unsaturated equatorial site of the Co center in side-on orientation (η^2-H_2) due to the proper orbital interaction and breaks the η^2-O=C or Co···H agostic interaction.

In **5La** or **5Ba**, H_2 occupies the equatorial site and the H−H bond lies in the basal plane in η^2-coordination. In comparison with the bond length (0.742 Å) of free H_2 or in the transition states (0.749/0.751 Å), the H−H distance is elongated (0.797 Å). At the same time, the $Co-C_{acyl}$ bond distance (2.040 vs 2.048 Å) is increased with respect to that in **4L-O** (1.877 Å) or **4B−O** (1.878 Å), which will facilitate the aldehyde elimination in the subsequent step. Our calculations illustrate that this addition process is endothermic by 24.8 and 30.3 kJ/mol for the linear (**5La**) and branched (**5Ba**) paths, and these results are supported by the experimental study by Sweany[59] on the photolysis of $(CH_3CO)Co(CO)_4$, indicating that $(CH_3CO)Co(CO)_3$ was remarkably stable even in the presence of H_2. In addition to the experimental study, a previous theoretical study[39] has predicted a similar energetic trend for the addition of H_2 to $(C_2H_5CO)Rh(PH_3)_2(CO)$.

Next, we paid attention to the dihydride complexes (**6L** and **6B**) and the paths of the oxidative addition reaction. As shown in Figures 7 and 8, **6L** and **6B** have six-coordinated octahedral geometries. Compared with the η^2 complexes **5La** and **5Ba**, the H−H distances in **6L** and **6B** are increased to 1.846 and 1.844 Å, respectively, accompanied with the shortening of the Co−H bonds. Because the substantial rotation of the acyl group emerges in the dihydride complexes (**6L** and **6B**) with respect to the η^2 adducts (**5La** and **5Ba)**, two pathways of oxidative addition can be conceived. One is the direct path from **5La** to **6L** or **5Ba** to **6B**. However, numerous attempts from our side to locate the transition states directly connecting the related species failed.

The alternative path is divided into two steps. First, the acyl group in **5La** (**5Ba**) rotates around the $Co-C_{acyl}$ bond through a corresponding transition state, **TS-(5La/5Lb)** or **TS(5Ba/5Bb)**, to **5Lb** (**5Bb**) without

(59) Sweany, R. L. *Organometallics* **1989**, *8*, 175.
(60) Pino, P.; Major, A.; Spindler, F.; Tannenbaum, R.; Bor, G.; Horváth, I. T. *J. Organomet. Chem.* **1991**, *417*, 65.

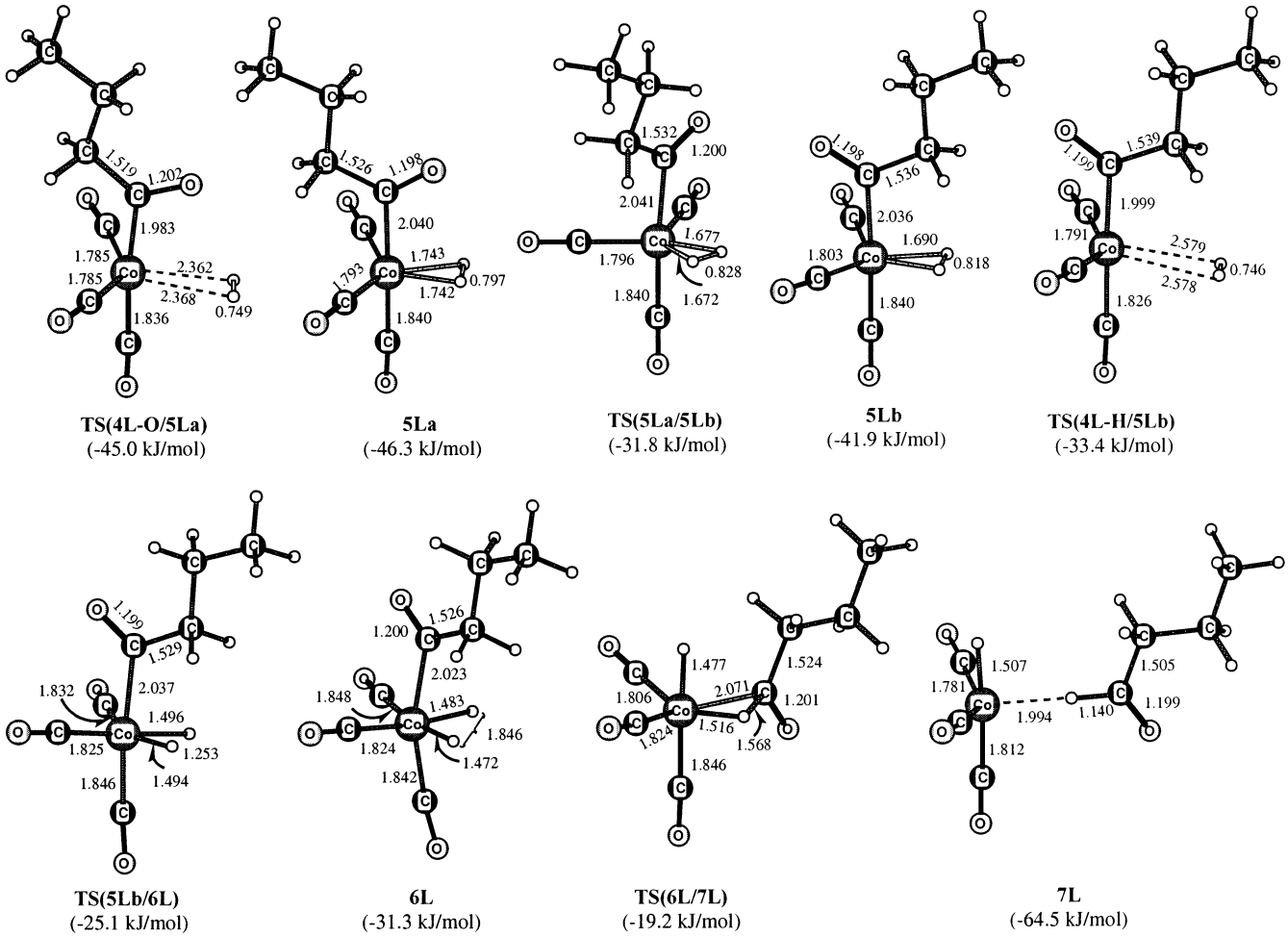

Figure 7. Bond parameters (Å) and relative energies for the intermediates and transition states of the H_2 oxidative addition and aldehyde elimination process for propyl (**L** for linear) substituent.

significant change of the H−H bond length during the rotation process. Our calculations show that the stable **5Lb** and **5Bb**, in which the acyl group rotates about 174.2° and 160.9° compared with **5La** and **5Ba**, are slightly higher in energy by 4.4 and 1.8 kJ/mol, respectively, and the rotation barriers are 14.5 and 12.0 kJ/mol.

Second, the H−H distance increases accompanied with a small rotation of the acyl group to form the dihydride complexes **6L** and **6B**. The related transition state structures for the H_2 oxidative addition, **TS(5Lb/6L)** and **TS(5Bb/6B)**, are depicted in Figures 7 and 8. The activation energies for **5Lb** to **6L** and **5Bb** to **6B** are 16.8 and 16.4 kJ/mol. In **TS(5Lb/6L)** and **TS(5Bb/6B)**, the H−H distances are elongated to 1.253 and 1.246 Å, and they are close to the average values of **5Lb** and **6L** or **5Bb** and **6B**. As a whole, the process of H_2 oxidative addition (**5La** to **6L** or **5Ba** to **6B**) is endothermic by 15.0 or 12.1 kJ/mol.

Following the H_2 oxidative addition process, the elimination reaction occurs, and the linear and branched aldehyde products are formed. Aldehyde elimination leads to the complexes **7L** and **7B**, in which the aldehyde coordinates with $HCo(CO)_3$ through the aldehyde hydrogen. The Co−H distance is 1.994 or 2.006 Å, and the C−H distance (1.140 or 1.141 Å) is longer than that in the free aldehyde *n*-C_3H_7CHO (1.113 Å) or *i*-C_3H_7CHO (1.114 Å). These values indicate that there is a weak agostic interaction between aldehyde and $HCo(CO)_3$ fragments. In addition, the elimination process proceeds via a three-center transition state, **TS(6L/7L)** or **TS(6B/7B)** (in Figures 7 and 8). The activation energies for the linear and branched aldehyde elimination processes are 12.1 and 9.0 kJ/mol, respectively.

In addition to the H_2 coordination to the acyl cobalt tricarbonyl complexes (**4L-H**/**4L-O** and **4B-H**/**4B-O**) for the formation of aldehydes, it is worth noting that the corresponding CO coordination is a potential competitive side reaction. There are two possible ways for CO to coordinate, one with the agostic acyl species **4L-H** or **4B-H**, and the other with η^2-O=C-stabilized **4L-O** or **4B-O**, and both channels lead to the same product, **5Lc** or **5Bc**. All the optimized structures and relative energies (relative to the sum of the energy of **1a-*syn*** and two CO) for the intermediates and transition states are shown in Figure 9. In contrast to the H_2 coordination process, this CO coordination process is highly exothermic by 66.0/55.2 and 59.1/51.1 kJ/mol for linear (**5Lc**) and branched (**5Bc**) paths, respectively, and the energy barriers are 18.9/9.4 kJ/mol for **TS(4L-H/5Lc)**/**TS(4L-O/5Lc)** and 20.1/12.5 kJ/mol for **TS(4B-H/5Bc)**/**TS(4B-O/5Bc)**.

(f) Entire Catalytic Cycle and Regioselectivity. Summarizing the results of each individual step discussed above, the entire PES for the propene hydro-

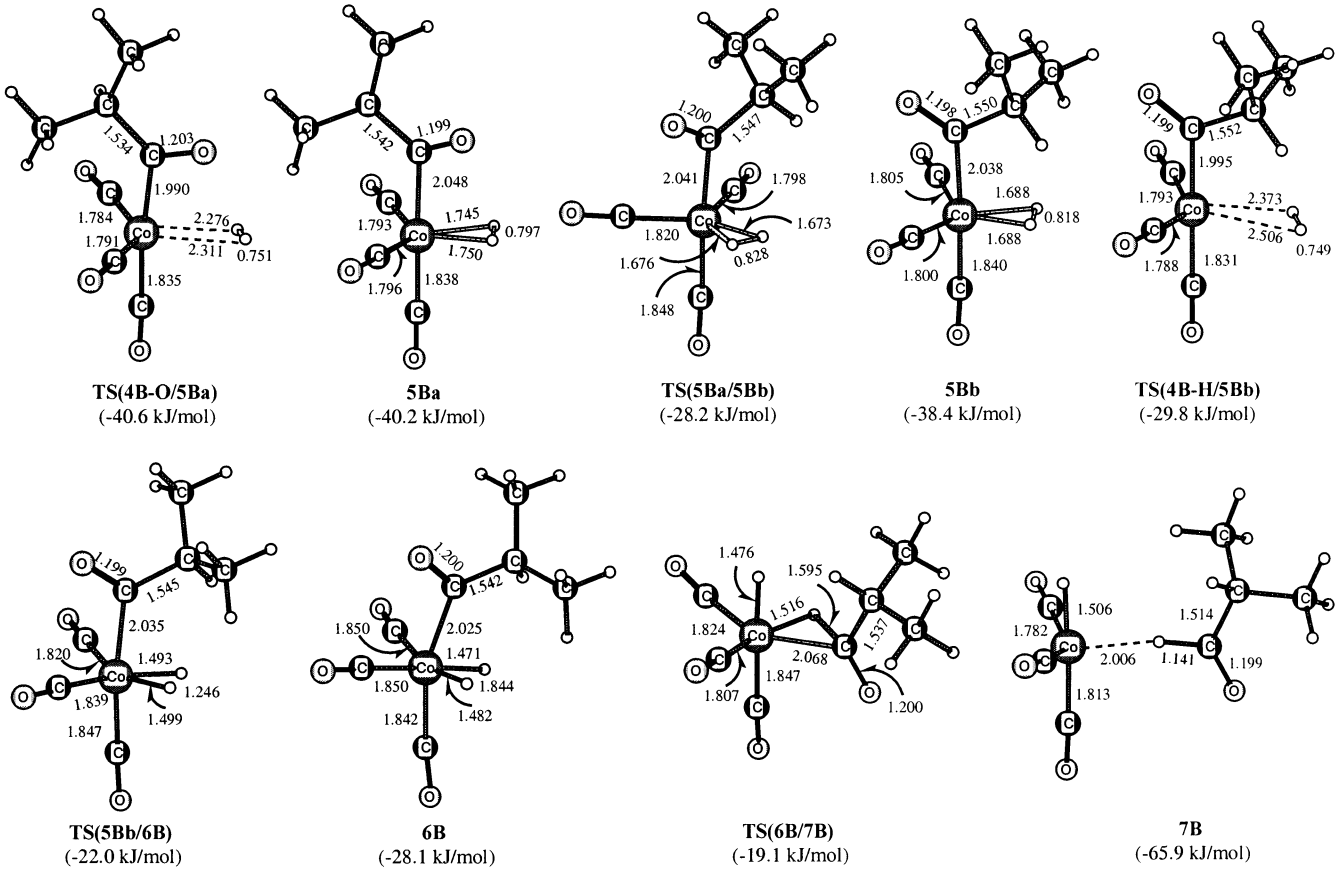

Figure 8. Bond parameters (in Å) and relative energies for the intermediates and transition states of the H_2 oxidative addition and aldehyde elimination process for isopropyl (**B** for branched) substituent.

formylation employing the active catalyst $HCo(CO)_3$ has been constructed and is displayed in Figure 10. The rate constants of each elementary reaction step were further computed at the typical reaction conditions of cobalt-catalyzed hydroformylation, 403.15 K and 200 atm. The calculated results of the rate constants as well as the activation energies and enthalpies of reaction are listed in Tables 1 and 2.

Before the discussion of the rate-determining step, it is worth analyzing the two possible channels of H_2 coordination, one from **4L-H/4B-H** to **5Lb/5Bb** and the other from **4L-O/4B-O** to **5La/5Ba**. As shown in Tables 1 and 2, both steps have very close rate constants, although those for the former are somewhat larger than for the latter, and they should be competitive.

For the linear pathway, the minor rate constants relate to the CO insertion (**3L** to **4L-H**) and the H_2 coordination (**4L-O** to **5La** or **4L-H** to **5Lb**) steps. Their rate constants have the same magnitudes (2.09×10^7 s^{-1}, 4.89×10^7 and 1.35×10^8 $s^{-1}\cdot mol^{-1}\cdot L$). It is noteworthy that the CO insertion is a unimolecular reaction, while the H_2 coordination is a bimolecular reaction. Therefore, the concentrations of **3L**, **4L-O**/**4L-H**, and H_2 impose a strong influence on the ratio of their reaction rates. It is also interesting to note that the CO coordination to the acyl complex (**4L-O**/**4L-H** to **5Lc**) owning the same magnitude of rate constants (1.90×10^7 and 5.48×10^7 $s^{-1}\cdot mol^{-1}\cdot L$) is competitive with the H_2 coordination (Table 1), which decreases the concentration of **4L-O**/**4L-H**. Additionally, the solubility of H_2 and CO in toluene is 0.322 and 1.125 mol/L at 403 K and 100 atm.[61] Considering all of these factors, either the CO insertion or the H_2 coordination can be the RDS under various reaction conditions.

For the branched pathway, however, the rate constant (5.89×10^7 s^{-1}) for the CO insertion step (**3B** to **4B-H**) is larger than that (1.25×10^6 and 3.99×10^6 $s^{-1}\cdot mol^{-1}\cdot L$) for the H_2 coordination (**4B-O** to **5Ba** or **4B-H** to **5Bb**). Competitive with the H_2 coordination is also the CO coordination (**4B-O**/**4B-H** to **5Bc**), as indicated by the rate constants (4.35×10^6 and 1.13×10^7 $s^{-1}\cdot mol^{-1}\cdot L$) in Table 2. Taking both the rate constant and the concentration effect into account, the CO insertion reaction is faster than the H_2 coordination. Thus, the H_2 coordination is the RDS of the entire catalytic cycle. In the deuterioformylation experiment, the inverse kinetic isotope effects supported the hydrogen atom transfer occurring before or during the RDS.[11] This showed that the RDS should be a reaction step involving H_2. On the other hand, the competitive coordination of CO and H_2 explains the observed effects of partial pressure, which influences the entire reaction rate and also the regioselectivity.

On the basis of the above relationship, the regioselectivity of propene hydroformylation employing the active catalyst $HCo(CO)_3$ will be discussed. As mentioned in the Introduction, there are a number of studies focused on the regiochemistry of Rh-catalyzed hydroformylation. Experimental evidence suggests that the regiochemistry of aldehyde formation is controlled by

(61) Gholap, R. V.; Kut, O. M.; Bourne, J. R. *Ind. Eng. Chem. Res.* **1992**, *31*, 1597.

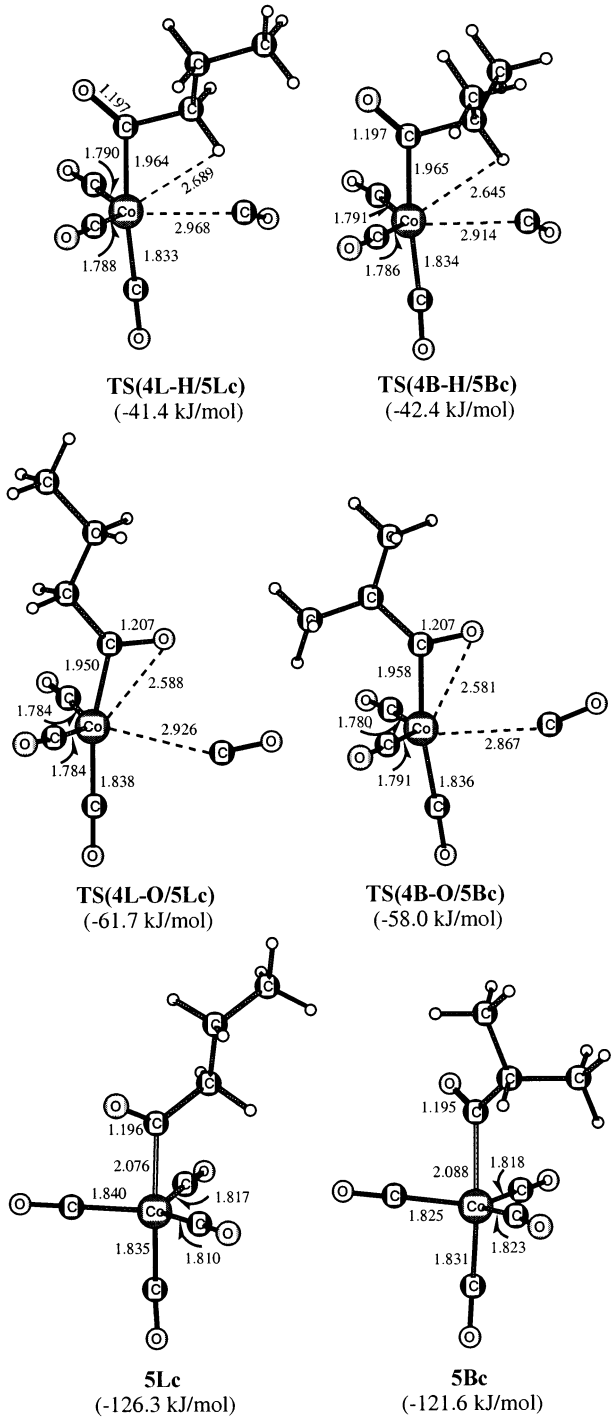

Figure 9. Bond parameters (in Å) and relative energies for the intermediates and transition states of CO addition to $(C_3H_7CO)Co(CO)_3$.

an irreversible olefin insertion for the rhodium-based catalysts.[24] However, much less is known about using cobalt catalysts.

From the large rate constants and low activation energies in Tables 1 and 2, the internal propene rotation and the propene insertion into the Co−H bond for both linear and branched reactions are rapid and reversible processes, but the subsequent CO additions to the linear and branched alkyl cobalt tricarbonyl complexes (**2L** and **2B**) are exothermic and irreversible. Therefore, the regioselectivity should be mainly controlled by the relative stability of the CO addition products (**3L** and **3B**). At B3LYP/6-311+G(d)*, **3L** is found more stable than **3B** by 8.6 kJ/mol, and this indicates that linear product is more favorable than the branched one. This energy difference is primarily caused by the steric interaction of the isopropyl group and the equatorial CO ligands in **3B** (Figure 6), and therefore the regioselectivity of Co-catalyzed hydroformylation is a thermodynamically controlled process.

The reversibility of the alkylation reaction reveals the observed isomerization between internal and terminal olefin and the H/D isotope exchange;[62] for example, hydroformylation of both terminal and internal olefins (1-pentene and 2-pentene) led nearly to the same ratio of linear to branched products. The best example for the observed isomerization of olefins is shown in Scheme 2. From 3-methyl-1-pentene (**A**), both the expected aldehydes (**I** and **II**) as the logical products were observed, but the unexpected product **IV** was also found. It is to be noted that aldehydes **II** and **IV** are the expected products of 3-methyl-2-pentene (**B**) and 2-ethyl butene (**C**).[62] This indicates the enhanced probability of olefin isomerization or double-bond shifts under the hydroformylation conditions.

We found that the thermodynamic stability of linear over branched alkyl cobalt tetracarbonyl from the irreversible and exothermic CO addition reaction is responsible for the observed regioselectivity. This conclusion is supported by the reactions of 3-methyl-2-pentene (**B**) and 2-ethyl butene (**C**), which gave only products **II** and **IV**, and the expected branched product **III** was not observed (Scheme 2). This can be ascribed to the stability of the corresponding alkyl tetracarbonyl complexes; for example, that of **IV** is a primary carbon, that of **II** is a secondary carbon, and that of **III** is a tertiary carbon. The most representative example of the steric effect is the hydrofromylation of isobutene, which gives a ratio of linear to branched aldehydes of 40:1.[62]

For a possible reaction carried out at 403 K, the regioselectivity of 93:7 for **3L** to **3B** is predicted. It is well known that the regioselectivity of olefin hydroformylation depends on many factors,[62] e.g., catalyst concentration, operating temperature, and partial pressure of CO and H_2. Considering the subtle influence of all these parameters, the calculated value agrees well with the experimental finding (around 80:20).[2]

At the end of our analysis, it is worth comparing our results with the available literature data from past decades for some of the individual steps. In case of the propene coordination, our investigation shows that the potential energy surface of the π-complex $HCo(CO)_3(\eta^2$-$H_2C{=}CHCH_3)$ is asymmetrical and the C=C bond perpendicular to the Co−H bond is the preferred coordination mode. A similar tendency for ethylene hydroformylation was predicted by Antolovic and Davidson using the ab initio CI//HF method[42] and by Versluis et al. based on the HFS model.[43]

In a previous study by Versluis et al.,[43] the ethylene insertion into the Co−H bond was explored at the HFS level. A linear transit procedure was adopted to approximate the energy profile for the migratory process under a C_s symmetry constraint. The activation energy

(62) For an excellent review, see: Cornils, B. *Hydroformylation. Oxo Synthesis, Roelen Reaction* in *New Sytheses with Carbon Monoxide*; Falbe, J., Ed.; Springer-Verlag: Berlin, 1980.

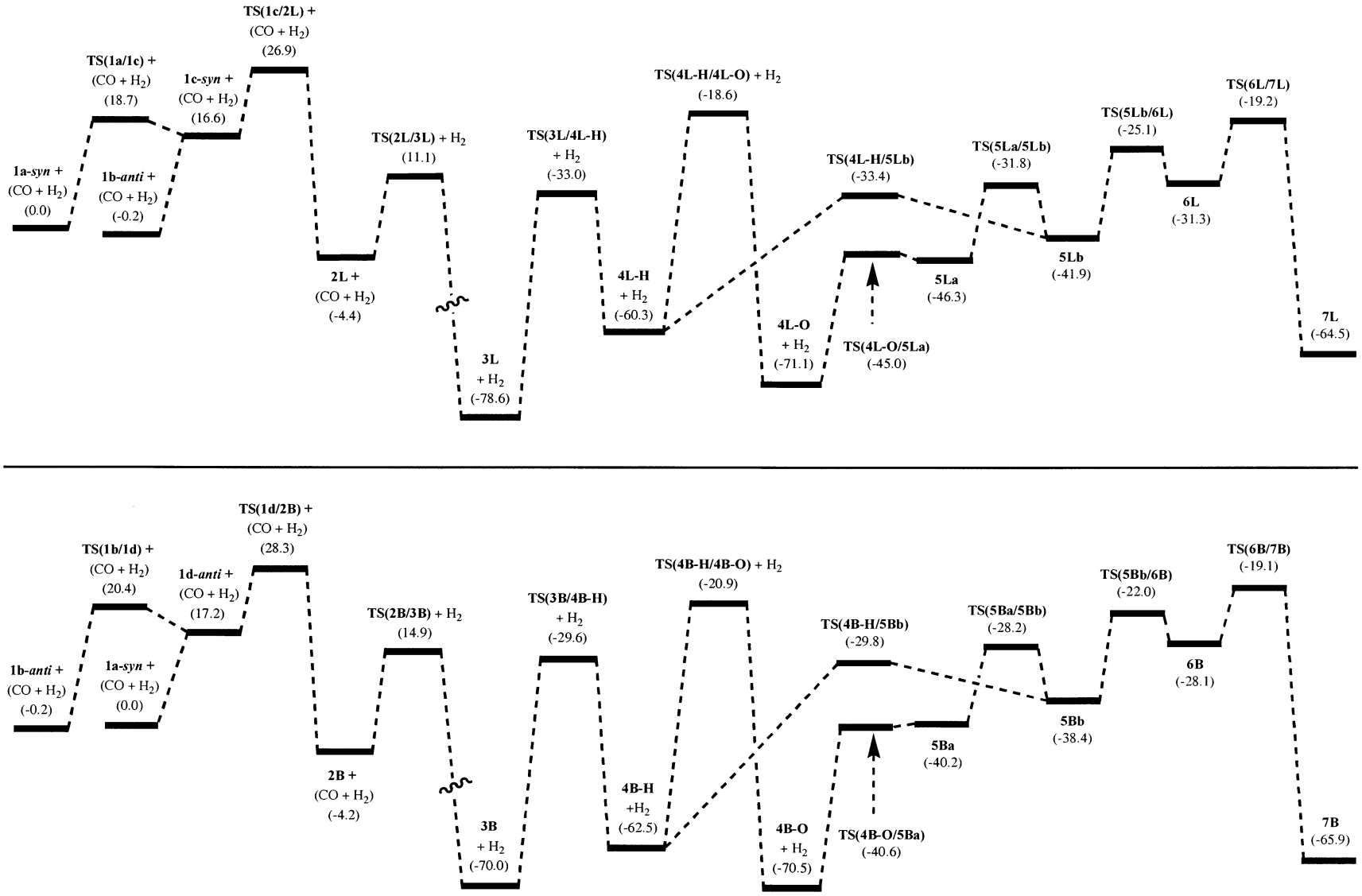

Figure 10. Potential energy profiles (in kJ/mol) for the linear (top) and branched (bottom) processes.

Table 1. Activation Energies ($\Delta E^{\ddagger}$, kJ/mol), Enthalpies of Reaction (ΔH, kJ/mol), and Reaction Rate Constants (k_i and k_{-i}, s^{-1} or $s^{-1}\cdot mol^{-1}\cdot L$) at 403.15 K and 200 atm for the Linear Pathway

no.	reaction	$\Delta E^{\ddagger a}$	ΔH^a	k_i	k_{-i}
	Olefin Insertion				
1L	**1b-*anti* → TS(1b/1c) → 1c-*syn***	16.8	16.8	2.30×10^{11}	8.40×10^{12}
1L′	**1a-*syn* → TS(1a/1c) → 1c-*syn***	18.7	16.6	1.26×10^{10}	4.64×10^{11}
2L	**1c-*syn* → TS(1c/2L) → 2L**	10.3	−21.0	1.40×10^{11}	9.88×10^{8}
	CO Addition and Insertion				
3L	**2L + CO → TS(2L/3L) → 3L**	15.5	−74.2	1.35×10^{9}	1.85×10^{4}
4L	**3L → TS(3L/4L-H) → 4L-H**	45.6	18.3	2.09×10^{7}	3.94×10^{9}
5L	**4L-H → TS(4L-H/4L-O) → 4L-O**	41.7	−10.8	7.79×10^{7}	1.25×10^{6}
	H_2 Coordination and Oxidative Addition				
6L	**4L-O + H_2 → TS(4L-O/5La) → 5La**	26.1	24.8	4.89×10^{7}	8.15×10^{13}
7L	**5La → TS(5La/5Lb) → 5Lb**	14.5	4.4	4.71×10^{9}	3.12×10^{10}
8L	**4L-H + H_2 → TS(4L-H/5Lb) → 5Lb**	26.9	18.4	1.35×10^{8}	2.39×10^{13}
9L	**5Lb → TS(5Lb/6L) → 6L**	16.8	10.6	1.26×10^{11}	3.72×10^{12}
	Aldehyde Reductive Elimination				
10L	**6L → TS(6L/7L) → 7L**	12.1	−33.2	1.20×10^{11}	2.94×10^{4}
	Side Reaction: CO Coordination to Acyl Complex				
S1L	**4L-H + CO → TS(4L-H/5Lc) → 5Lc**	18.9	−66.0	1.90×10^{7}	2.54×10^{3}
S2L	**4L-O + CO → TS(4L-O/5Lc) → 5Lc**	9.4	−55.2	5.48×10^{7}	4.58×10^{5}

[a] At B3LYP/6-311+G(d)* + ZPE (B3LYP/6-311+G(d)*).

Table 2. Activation Energies ($\Delta E^{\ddagger}$, kJ/mol), Enthalpies of Reaction (ΔH, kJ/mol), and Reaction Rate Constants (k_i and k_{-i}, s^{-1} or $s^{-1}\cdot mol^{-1}\cdot L$) at 403.15 K and 200 atm for the Branched Pathway

no.	reaction	$\Delta E^{\ddagger a}$	ΔH^a	k_i	k_{-i}
	Olefin Insertion				
1B	**1a-*syn* → TS(1a/1d) → 1d-*anti***	17.2	17.2	1.97×10^{11}	8.40×10^{12}
1B′	**1b-*anti* → TS(1b/1d) → 1d-*anti***	20.6	17.4	7.11×10^{9}	3.01×10^{11}
2B	**1d-*anti* → TS(1d/2B) → 2B**	11.1	−21.4	1.34×10^{11}	9.30×10^{8}
	CO Addition and Insertion				
3B	**2B + CO → TS(2B/3B) → 3B**	19.1	−65.8	1.21×10^{8}	4.47×10^{4}
4B	**3B → TS(3B/4B-H) → 4B-H**	40.4	7.5	5.89×10^{7}	3.28×10^{8}
5B	**4B-H → TS(4B-H/4B-O) → 4B-O**	41.6	−8.0	5.82×10^{7}	2.08×10^{6}
	H_2 Coordination and Oxidative Addition				
6B	**4B-O + H_2 → TS(4B-O/5Ba) → 5Ba**	29.9	30.3	1.25×10^{6}	4.08×10^{13}
7B	**5Ba → TS(5Ba/5Bb) → 5Bb**	12.0	1.8	3.12×10^{10}	2.43×10^{10}
8B	**4B-H + H_2 → TS(4B-H/5Bb) → 5Bb**	32.7	24.1	3.99×10^{6}	3.70×10^{12}
9B	**5Bb → TS(5Bb/6B) → 6B**	16.4	10.3	6.36×10^{10}	2.44×10^{12}
	Aldehyde Reductive Elimination				
10B	**6B → TS(6B/7B) → 7B**	9.0	−37.8	3.98×10^{11}	1.61×10^{4}
	Side Reaction: CO Coordination to Acyl Complex				
S1B	**4B-H + CO → TS(4B-H/5Bc) → 5Bc**	20.1	−59.1	4.35×10^{6}	5.41×10^{3}
S2B	**4B-O + CO → TS(4B-O/5Bc) → 5Bc**	12.5	−51.1	1.13×10^{7}	3.94×10^{5}

[a] At B3LYP/6-311+G(d)* + ZPE (B3LYP/6-311+G(d)*).

Scheme 2. Hydroformylation of 3-Methyl-1-pentene, 3-Methyl-2-pentene, and 2-Ethyl butene

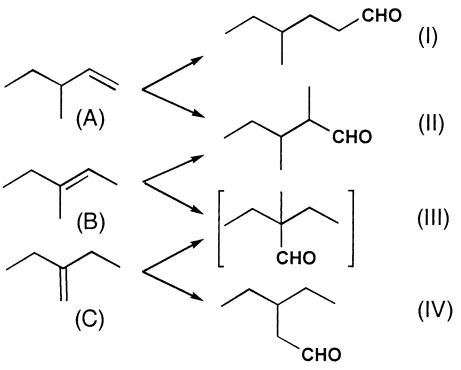

was predicted to be 6 kJ/mol, although the corresponding transition state was not located. However, our investigation reveals that the olefin insertion reaction does not occur on a C_s symmetry potential energy surface. An interesting feature of the olefin insertion is that after the transition state the hydride migration is accompanied by a simultaneous Berry pseudorotation leading to the Co···H−C agostic stabilized (iso)propyl complex with the (iso)propyl group at the axial site. The isomer with the (iso)propyl group at the equatorial site is not a minimum structure. For the alkyl species $(C_2H_5)Co(CO)_3$, Versluis et al.[43] found that the two above geometries were energy minimum structures, and the isomer with the ethyl group in the equatorial position was higher in energy. However, Antolovic and Davidson[42] obtained the opposite conclusion based on the CI//HF calculations. This is due to the limitation of the HF method to describe such Co···H−C agostic interactions.

Employing hydrogen or methyl as the alkyl model, the CO insertion reaction has been investigated by the HF[42] and HFS[45] methods. At the HFS level, Versluis et al.[45] studied the insertion process occurring on the C_s symmetry potential energy surface. However, this result is not supported by the recent B3LYP calculations by Goh and Marynick[46] and our new findings. Instead of a single-step process, the carbonylation reaction occurs via

two pseudorotated transition states and a Co···H−C agostic stabilized intermediate, originated from the frontier orbital interactions.

For the H_2 coordination to the unsaturated acyl complex, our calculations illustrate that it is an endothermic process by 24.8 and 30.3 kJ/mol for the linear (**4L-O** to **5La**) and branched (**4B-O** to **5Ba**) paths, respectively. This finding is in contrast to that of Ziegler's results. They found that the H_2 coordination reaction is nearly thermoneutral with a calculated reaction enthalpy of −2 kJ/mol at the HFS level,[47] or an exothermic process that releases 10.5 kJ/mol at the BP86 level.[48] To verify this difference, we have repeated their calculations with the same model ($(CH_3CO)Co(CO)_3 + H_2$) using our method. The endothermic result by 23.6 kJ/mol is similar to that for **4L-O** or **4B-O**. Moreover, as previously mentioned, our results are supported by the experimental study of Sweany[59] and by the relevant theoretical study for the addition of H_2 on $(C_2H_5CO)Rh(PH_3)_2(CO)$.[39] Thus, our results should be reasonable.

Conclusion

The potential energy surface of the full catalytic cycle of propene hydroformylation employing $HCo(CO)_3$ as an active catalyst has been investigated at the B3LYP/6-311+G(d)* level. The reported theoretical study is of significant interest for the industrially important hydroformylation of higher olefins (predominantly the C8/C9 range from feedstock), which is performed on a million-ton scale per year in the presence of cobalt carbonyl complexes.

All species involved in the catalytic cycle have been fully characterized to be energy minimum structures for the intermediates or saddle point structures for the transition states. The most stable propene π complex ($HCo(CO)_3(\eta^2\text{-}H_2C{=}CHCH_3)$) has the C=C double bond perpendicular to the Co−H bond, while the isomer with the C=C double bond parallel to the Co−H bond is higher in energy due to the orbital interaction and the steric effect. It is found that the insertion between Co−H and C=C goes through a migratory insertion transition state, accompanied by a simultaneous rotation of the $Co(CO)_3$ group, leading to the stable alkyl complex with the (iso)propyl group at the axial position ($((C_3H_7)Co(CO)_3$) and stabilized by an additional Co···H−C agostic interaction at the formally vacant equatorial position. The interaction between Co−H and C=C is electronic rather than electrostatic, in contrast to the previous speculation. The alkylation process is reversible, because both forward and reverse reactions have small activation energies, and therefore does not control the regioselectivity in favor of the linear product. This reversible process reveals the observed isomerization process between internal and terminal olefins.

However, the subsequent CO addition to the alkyl complex ($RCo(CO)_3 + CO = RCo(CO)_4$) has a small activation energy and is very exothermic, and the relative stability of the corresponding linear and branched complexes $RCo(CO)_4$ should be responsible for the regioselectivity, which is a thermodynamically controlled process. Our computations show that the formation of the linear product is more favored than the branched one. This reasonably explains the observed product distribution in Scheme 2.

The CO insertion (carbonylation) leading to the most stable acyl complex, $(RCO)Co(CO)_3$, in which the acyl group is at the axial position with the O=C oxygen facing the vacant equatorial site to form the stable η^2 interaction, goes through two steps: (i) the alkyl migration to the equatorial CO bond, accompanied by a simultaneous $Co(CO)_3$ rotation after the transition state for the formation of the Co···H−C agostic stabilized acyl complex; (ii) the further rotation of the $Co(CO)_3$ group with the breaking of the agostic interaction resulting in the more stable η^2-O=C stabilized acyl complex. The computed characteristic vibrational modes of the η^2-O=C acyl complex agree with experimental findings, and this in turn identifies the η^2-O=C acyl complex to be more stable than the agostic one, in line with our calculations.

Furthermore, the η^2-O=C acyl complex was found experimentally to be stable toward H_2 addition, which is computed to be an endothermic process. On the basis of the computed reaction rates for each elementary step, the rate-determining step is H_2 coordination to the agostic or η^2-O=C acyl complexes rather than the normally suggested H_2 oxidative addition.

Acknowledgment. This paper is dedicated to Prof. G. Oehme (Ifok, Rostock) on the occasion of his 65th birthday. This work was supported by the Chinese Academy of Sciences (20029908) and the National Natural Science Foundation China.

Supporting Information Available: Total electronic energies and zero-point energies (ZPE) as well as thermal correction to enthalpies and thermal correction to Gibbs free energies (403.15 K, 200 atm) for all systems. Some selected natural charges and vibration frequencies are collected. This material is available free of charge via the Internet at http://pubs.acs.org.

OM0304863